

BABE: Biology Arena BEnchmark

Junting Zhou^{1,2,*}, Jin Chen^{1,*}, Linfeng Hao^{2,*}, Denghui Cao^{1*}, Zheyu Wang¹,
 Qiguang Chen¹, Chaoyou Fu¹, Jiaze Chen¹, Yuchen Wu¹, Ge Zhang¹, Mingxuan
 Wang^{1,†}, Wenhao Huang^{1,†}, Tong Yang^{2,†}

¹ByteDance Seed, ²Peking University

*Work done at ByteDance Seed, [†]Corresponding authors

Abstract

The rapid evolution of large language models (LLMs) has expanded their capabilities from basic dialogue to advanced scientific reasoning. However, existing benchmarks in biology often fail to assess a critical skill required of researchers: the ability to integrate experimental results with contextual knowledge to derive meaningful conclusions. To address this gap, we introduce **BABE** (Biology Arena BEnchmark), a comprehensive benchmark designed to evaluate the experimental reasoning capabilities of biological AI systems. BABE is uniquely constructed from peer-reviewed research papers and real-world biological studies, ensuring that tasks reflect the complexity and interdisciplinary nature of actual scientific inquiry. BABE challenges models to perform causal reasoning and cross-scale inference. Our benchmark provides a robust framework for assessing how well AI systems can reason like practicing scientists, offering a more authentic measure of their potential to contribute to biological research.

Date: February 6, 2026

Correspondence: Junting Zhou at juntingzhou@stu.pku.edu.cn; Tong Yang at yangtong@pku.edu.cn

1 Introduction

The evolution of large language models (LLMs) has witnessed a paradigm shift from basic conversational capabilities to advanced reasoning functionalities. Early-generation models excelled at generating coherent chat-style responses, but modern foundation models have expanded into **scientific research capabilities**—including hypothesis generation, data analysis, and experimental design. This shift has drawn significant attention to evaluating LLMs' performance in specialized scientific domains, particularly biology, where complex experimental data and interdisciplinary knowledge demand more than trivial pattern recognition.

A critical yet underdeveloped aspect of assessing biological AI systems is their ability to reason based on experimental results and contextual background, which is a core skill for biological researchers. For instance, interpreting a Western blot image to infer protein expression changes requires integrating visual data (for example: band intensity, loading controls) with experimental context (for example: treatment conditions, cell lines) and domain knowledges. This kind of problem is a challenge even for the strongest current SOTA models.

However, existing benchmarks rarely test this integrated reasoning ability, instead focusing on isolated tasks like sequence classification or structure prediction.

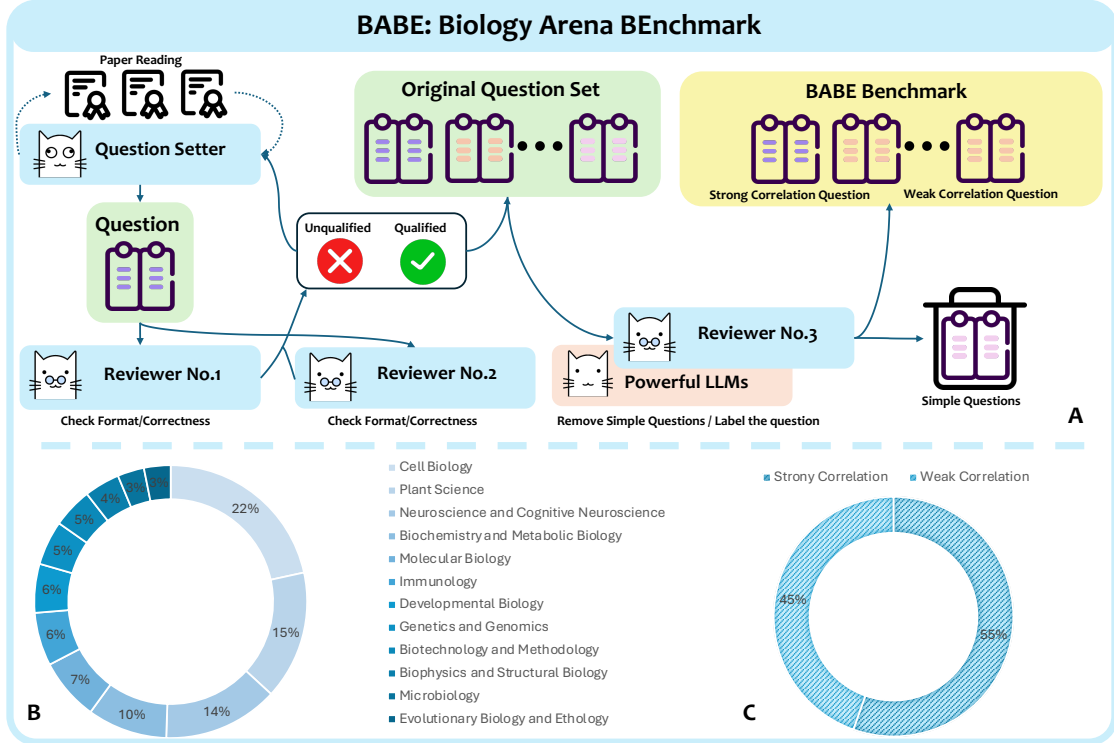


Figure 1 Overview of the BABE (Biology Arena BEnchmark) construction and composition. (A) The multi-stage annotation pipeline for constructing the BABE benchmark. (B) The disciplinary distribution of questions in the BABE benchmark, covering 12 subfields of biology. (C) The proportion of strong-correlation (45%) and weak-correlation (55%) questions in the final BABE benchmark.

To address these gaps, we develop BABE(Biology Arena BEnchmark1), a benchmark specifically designed to evaluate biological AI systems' experimental reasoning capabilities. Critically, all tasks in **BABE** are derived from peer-reviewed research papers and real-world biological studies. This ensures that the benchmark reflects the true complexity of biological research and tests models' ability to reason like practicing scientists.

In summary, Our work makes three primary contributions:

- **Experimental Reasoning Focus:** Unlike existing benchmarks, BABE centers on tasks that require models to integrate experimental results with contextual background to derive biological conclusions.
- **High-Difficulty, Research-Derived Tasks:** All tasks are adapted from peer-reviewed papers and designed to demand causal reasoning and cross-scale inference.
- **Broad Domain Coverage:** We cover major biological domains, using tasks from diverse subfield studies, enabling evaluation of model generalization across real-world biological research areas.

2 Related Work

2.1 Deep Research Agents

The initial success of Large Language Models (LLMs) in natural language tasks was often hampered by inherent limitations in multi-step reasoning, knowledge cut-offs, and the propensity for hallucination [4]. This motivated a critical shift from static generation toward the development of sophisticated Deep Research Agents. These agents are designed to tackle complex, multi-turn informational research tasks by equipping the LLM core with a structured control loop, thereby enabling dynamic reasoning, adaptive long-horizon planning, multi-hop information retrieval, iterative tool use, and the generation of structured analytical

reports [2, 17, 20].

The introduction of agency relies on three primary functional pillars: (1) Planning and Control, typically achieved through mechanisms like iterative planning and self-reflection to maintain task alignment and correct errors [9]; (2) External Tool Utilization, encompassing code interpreters, specialized APIs, and web search to access computational and real-time resources [14]; and (3) Contextual Grounding, most commonly implemented via Retrieval-Augmented Generation (RAG) [7] to seamlessly incorporate up-to-date or proprietary domain-specific data. This composite framework allows agents to interact dynamically with complex environments and accumulate long-term memory, thereby achieving sustained logical reasoning and verifiable evidence retrieval necessary for accelerated research, literature review synthesis, and scientific hypothesis generation.

However, evaluating the true scientific utility of these systems remains a significant challenge. Crucially, the effective assessment of these domain-specific agents, particularly in high-stakes fields like Biology and Medicine, necessitates challenging benchmarks that test deep comprehension, multi-step causal reasoning, and faithful evidence extraction over highly specialized and voluminous literature [8], moving beyond general knowledge assessment.

2.2 Scientific Benchmarks

General scientific benchmarks have emerged to evaluate AI systems across disciplines like physics, chemistry, and biology [10, 12, 23], with a focus on testing domain knowledge and problem-solving skills. Initial efforts focused on high-difficulty, factual question-answering, exemplified by **GPQA** [13] and its scaled successor **SuperGPQA** [15], which feature expert-authored, graduate-level questions. Other highly challenging benchmarks include **HLE** [11], which assesses advanced STEM and humanities through short-answer and multimodal tasks, and **R-Bench** [19], which targets Graduate/Olympiad-level reasoning using bilingual, multimodal inputs. Furthermore, **SciEval** [18] aggregates academic datasets for broad STEM coverage, while **OlympicArena** [3] evaluates multidisciplinary cognitive reasoning with a focus on process-level assessment.

2.3 Biology-Specific Benchmarks

Biology-specific benchmarks have focused on subfield-specific tasks, but few address the integrated experimental reasoning that is critical for advancing the field. Table 1 summarizes key biology benchmarks and their limitations relative to **BABE**. Several benchmarks are Sequence-Centric. For example, benchmarks like Biology-Instructions [1] and ProteinBench [21] focus on sequence-based tasks (e.g., DNA sequence alignment, protein secondary structure prediction). Understanding structures of Bio-macromolecules is a crucial task in biology. Hence, there are Structure-Centric Benchmarks, especially in protein area. For example, ProteinShake [6] and PepPCBench [22] evaluate models on protein structure, using PDB-formatted structures to assign proteins to fold families. While these benchmarks are valuable for assessing structural biology models [5], they do not require models to interpret experimental data related to structures. Meanwhile, there is a small number of biology benchmarks incorporate multiple modalities, but they lack the depth of experimental reasoning required for real research. For example, BioASQ [16] organizes challenges on biomedical semantic indexing and question answering relevant to hierarchical text classification, machine learning, information retrieval, QA from texts and structured data, multi-document summarization and many other areas. OlymBench is a new benchmark designed to evaluate the reasoning ability of large language models, with challenges reaching competition difficulty. All existing biology-specific benchmarks fail to address one or more critical needs:

- Real experimental data: Most use simplified data or summarized data rather than figures and datasets from published papers.
- Integrated reasoning: Tasks do not require linking experimental results to contextual background;
- Broad domain coverage: Benchmarks are limited to single subfields rather than spanning multiple biological domains.

BABE addresses these gaps by focusing on research-derived, multimodal tasks that require the same reasoning as practicing biologists.

Table 1 Key Biology Benchmarks and their Gaps Relative to **BABE**

Benchmark	Real Experimental Data	Integrated Reasoning	Domain Coverage	Primary Focus
ProteinBench	No	Limited	Narrow	Computational Metrics
ProteinShake	No	Limited	Narrow	Standardized Structural Data
PepPCBench	No	Limited	Narrow	Structure Prediction Accuracy
BioASQ	No	Medium	Broad	Text/Sequence QA Corpus
OlymBench	No	High	Broad	High-difficulty Logical Deduction
BABE	Yes	High	Broad	Research-Derived Multimodal Tasks

3 Approach

3.1 Problem Formulation

The **Biology Arena Benchmark (BABE)** is introduced as a novel diagnostic framework designed to rigorously evaluate Large Language Models (LLMs) on complex reasoning tasks within the biomedical domain, specifically over a single source research document D . Unlike existing benchmarks, which often emphasize factual recall or single-hop retrieval, fail to fully diagnose model robustness in *compositional reasoning*, our benchmark focus on handling the complexity and quantitative content inherent in scientific literature. BABE addresses this limitation by defining a structured question triplet:

$$Q_{\text{BABE}} = \{Q_1, Q_2, Q_3\},$$

where the logical relationship between consecutive questions, $R(Q_i, Q_{i+1})$, is formally classified into two distinct diagnostic categories: **Strong Correlation** (R_{Strong}) and **Weak Correlation** (R_{Weak}). This structured methodology is essential for precisely measuring LLM *depth* (sequential inference) and *breadth* (parallel extraction) of understanding in a domain-specific context.

The problem formulation is centered on the interdependency within the question set Q_{BABE} . The overall type of a benchmark instance is defined by the combined logical relations:

$$Q_{\text{BABE}}^{\text{Type}} \equiv R(Q_1, Q_2) \wedge R(Q_2, Q_3).$$

The **Strong Correlation** relation (R_{Strong}) captures sequential, multi-hop reasoning, where the derived output of a preceding question is a necessary input for the subsequent one. This relationship is formally defined as:

$$R_{\text{Strong}} \Leftrightarrow \forall i, j (i < j), A_j \text{ requires } A_i \text{ for optimal derivation from } D.$$

Conversely, the **Weak Correlation** relation (R_{Weak}) captures parallel, independent extraction, where questions are logically uncoupled, testing the model's ability to maintain multiple distinct contexts simultaneously. This is formalized as:

$$R_{\text{Weak}} \Leftrightarrow \exists C_i \subset D \text{ s.t. } A_i = \text{Extract}(C_i), \text{ and } \forall i \neq j, C_i \cap C_j \approx \emptyset.$$

The formal constraint of R_{Strong} diagnoses failure modes related to error propagation and reasoning drift in *Chain-of-Thought (CoT)* processes, while R_{Weak} diagnoses issues such as semantic interference during simultaneous knowledge retrieval.

3.2 Data Collection

To construct a high-quality benchmark tailored for rigorous evaluation of domain-specific reasoning, we adopted a multi-stage data collection pipeline integrating frontier literature curation, expert-driven item development, and structured quality assurance.

As shown in 1(A), We first curated a corpus of cutting-edge scientific materials, including recently published peer-reviewed papers, domain-specific monographs, and authoritative review articles. The selection criteria

emphasized (i) recency of publication, (ii) relevance to the target scientific domain, and (iii) conceptual depth suitable for assessing multi-step reasoning. Only sources meeting all criteria were retained for downstream question construction.

For each selected paper or book chapter, domain experts generated a set of three assessment items. The items were designed to probe different cognitive dimensions, including conceptual understanding, methodological interpretation, and higher-order reasoning. All questions were required to be self-contained, unambiguous, and faithful to the source material while avoiding superficial fact-retrieval prompts.

A secondary panel of senior experts conducted a rigorous review of all drafted items. The review served two purposes:

- **Relevance Assessment:** Each question was labeled as either strong correlation or weak correlation to the core knowledge unit extracted from the source text. Strongly related questions directly test key concepts and reasoning chains presented in the material, whereas weakly related questions assess peripheral or contextual understanding.
- **Correctness Verification:** Reviewers evaluated the factual fidelity, logical coherence, and answer correctness for every item.

Items passing both relevance assessment and correctness verification were accepted into the benchmark. Items found to contain factual inaccuracies, ambiguous phrasing, or misalignment with the source were returned to the original authors for revision. After revision, questions underwent a second-round review before being considered for final inclusion. With the help of LLMs, simple questions were removed by the reviewers in this round.

Only items that successfully completed the full development–review–revision cycle were incorporated into the released benchmark. This multi-layered pipeline ensures that the dataset captures high-quality, expert-vetted questions with explicit relevance annotations, enabling more fine-grained evaluation of model capabilities across varying levels of semantic alignment with the underlying scientific sources.

4 Experiments

4.1 Overall Performance Analysis

Table 2 Model Performance on BABE Comparison

Model Name	Average Score	Strong Correlation	Weak Correlation
OpenAI-GPT-5.1-high	52.31	51.79	52.86
Gemini-3-Pro-Preview-Exp	52.02	49.05	55.16
OpenAI-o3-high.code	51.62	51.22	52.05
Doubao-1.8-1228	43.27	43.38	43.16
Gemini-2.5-Pro	42.17	42.02	42.33
Claude-Sonnet-4.5-thinking-azure	41.93	41.94	41.91
Doubao-1.6-1015-high.foreval	39.84	40.70	38.94
Doubao-1.6-thinking-0715.foreval	39.54	39.67	39.40
Doubao-1.6-1015-high.foreval (A)	39.34	35.10	43.81
Claude-Opus-4.1-thinking-azure	37.35	36.30	38.46
OpenAI-gpt4.1-0414	36.86	32.61	41.34
Doubao-1.6-1015-high.foreval (B)	36.64	34.88	38.49
QwenAPI-vl-max.latest	32.81	32.89	32.72
Doubao-1.5-pro-thinking.vision.0428.eval	31.71	32.12	31.28
Claude-Sonnet-4.5-nothinking-azure	31.66	33.67	29.55
QwenAPI-3-max-0923	26.54	27.70	25.32
GPT4o-1120	23.93	20.80	27.22
Doubao-1.6-flash.0828.foreval	22.04	20.34	23.83
GLM-4.5-V	20.83	18.09	23.72

Table 2 presents a comprehensive comparison of different models on the BABE benchmark under both strong and weak correlation settings. Overall, **OpenAI-GPT-5.1-high** achieves the best performance, obtaining the highest average score of **52.31**, and demonstrating consistently strong results across both strong (51.79) and weak (52.86) correlation subsets. This indicates robust reasoning capabilities that generalize well across varying dependency structures.

Models in the lower performance tier generally struggle with both correlation settings, with notable variations. For example, **OpenAI-gpt4.1-0414** (36.86) performs better in weak correlation (41.34) than strong correlation (32.61), while **Claude-Sonnet-4.5-nothinking-azure** (31.66) shows the opposite trend (33.67 for strong correlation vs. 29.55 for weak correlation), indicating divergent design trade-offs in handling explicit vs. implicit reasoning. The lowest-performing models, such as **GLM-4.5-V** (20.83) and **Doubao-1.6-flash.0828.foreval** (22.04), score consistently low across both subsets, suggesting fundamental limitations in reasoning capabilities for the BABE benchmark’s task requirements.

4.2 Strong vs. Weak Correlation

We observe notable performance differences between strong and weak correlation scenarios for several models. For example, **Gemini-3-Pro-Preview-Exp** exhibits a clear advantage under weak correlation conditions (55.16), substantially outperforming its strong correlation score (49.05). This suggests that the model is particularly effective when explicit logical dependencies are reduced, potentially benefiting from broader contextual reasoning. In contrast, models such as **Claude-Sonnet-4.5-thinking-azure** and **Gemini-2.5-Pro** show highly balanced performance across the two settings, indicating stable behavior regardless of correlation strength.

4.3 Reasoning Behavior Analysis on BABE

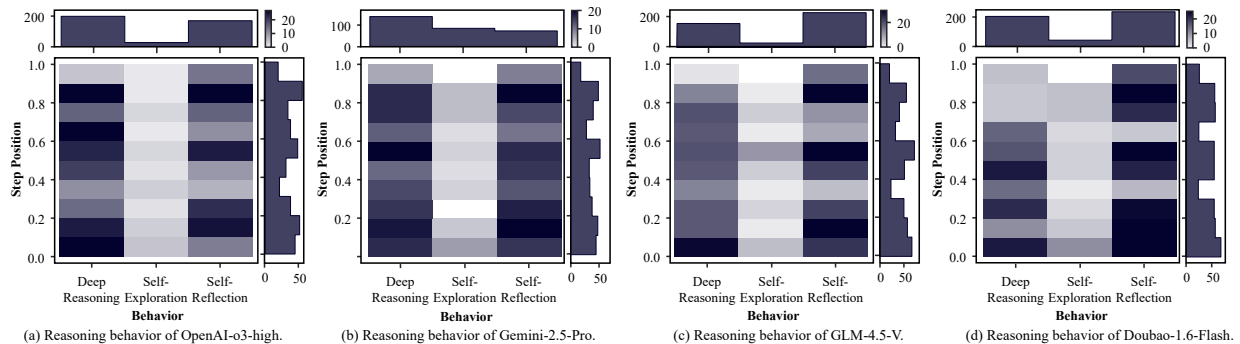


Figure 2 The Reasoning Behavior Distribution on BABE across four LLMs.

BABE requires deeper reasoning. To better understand the reasoning demands of BABE, we compare models at the two extremes of performance: the two best-performing models and the two worst-performing models. Figure 2 shows a clear association between success on BABE and the prevalence of Deep Reasoning behaviors during inference. Specifically, higher-performing models devote a substantially larger portion of their inference steps to deep reasoning, whereas lower-performing models exhibit a much smaller share of such behaviors. This pattern indicates that BABE is not primarily solved by shallow pattern matching; instead, it rewards deeper reasoning that resolves implicit or non-trivial dependencies in the input.

Excessive self-reflection on BABE can lead to a substantial degradation in reasoning performance. Figure 2 also reveals a second, more subtle failure mode among the worst-performing models: they exhibit episodic Self-Reflection at a notably higher rate, often exceeding their own proportion of deep reasoning. While limited self-reflection can be beneficial, these results suggest that frequent, repeated self-reflection without commensurate progress in deep reasoning is associated with worse outcomes on BABE. A plausible interpretation is that weaker models fall into an “overthinking” loop—spending many steps reconsidering intermediate thoughts or reformulating the approach—yet failing to advance the core reasoning needed to

reach correct conclusions. In practice, this behavior consumes the inference budget and increases the chance of drifting away from relevant evidence on BABE, which ultimately harms accuracy.

Strong performance on BABE depends on sustained, evenly applied deep reasoning. Beyond overall proportions, we observe that strong models tend to maintain deep reasoning consistently throughout the inference trajectory. In contrast, some models may begin with deep reasoning but gradually reduce such behaviors later in the process, yielding a sparser and less stable reasoning pattern. Figure 2 suggests that this “early burst” is insufficient for BABE: correctly solving BABE examples often requires repeatedly revisiting earlier premises, integrating newly derived implications, and maintaining coherent multi-step constraints until a final decision is justified. Therefore, strong performance on BABE depends not only on initiating deep reasoning, but on sustaining it in a relatively uniform manner across the full inference process.

4.4 Convergence Score Analysis

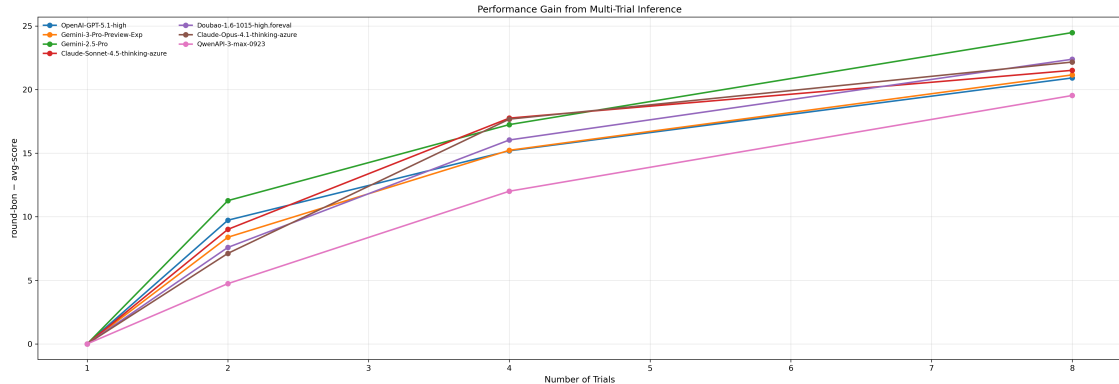


Figure 3 Performance gain from multi-trial inference.

We define the gain of multi-trial inference as:

$$\text{Gain}(n) = \text{model-BoN}(n) - \text{avg-score}(n),$$

where *BoN* is short for "Best of N", n denotes the number of inference trials. This metric isolates the improvement obtained purely from repeated sampling and aggregation, independent of the model’s average single-run performance.

To estimate the saturation behavior of gain, we fit a parametric saturating function:

$$\text{Gain}(n) = a \cdot (1 - e^{-bn}),$$

where a represents the asymptotic (converged) gain and b controls the convergence speed. Parameters are estimated using nonlinear least squares on observed gains at $n = \{1, 2, 4, 8\}$.

Figure 3 shows the gain achieved by increasing the number of inference trials. All models exhibit a monotonic increase in gain, confirming that multi-trial inference consistently improves performance beyond expected single-run outcomes. However, the slope of the curves decreases as n grows, indicating diminishing marginal returns and the onset of convergence.

Strong reasoning models such as **OpenAI-GPT-5.1-high** and **Gemini-3-Pro-Preview-Exp** exhibit relatively fast convergence, with predicted asymptotic gains around 30 points. These models show limited additional improvement beyond a moderate number of trials, suggesting that their reasoning quality is already robust in single or few-shot inference.

In contrast, several mid-tier models (e.g., **Gemini-2.5-Pro** and **Claude-Opus-4.1-thinking-azure**) display higher estimated gain limits, exceeding 35 points. This indicates greater diversity in their generated reasoning trajectories, allowing aggregation to recover substantially better solutions despite weaker average performance.

Trial	OpenAI-GPT-5.1		Gemini-3		Gemini-2.5-pro		Claude-S-4.5		Doubao-1.6		Claude-O-4.1	
	Avg	BoN	Avg	BoN	Avg	BoN	Avg	BoN	Avg	BoN	Avg	BoN
1	52.31	52.31	52.02	52.02	42.17	42.17	41.93	41.93	39.84	39.84	37.35	37.35
2	54.14	63.87	54.16	62.55	45.06	56.33	43.18	52.19	36.70	46.29	37.03	44.15
4	53.87	69.06	54.32	69.55	45.14	62.39	42.23	59.99	37.00	53.04	37.31	54.99
8	55.09	76.01	53.59	74.75	45.14	69.63	42.60	64.12	37.58	59.97	36.35	58.52
Convergence	–	81.90	–	86.54	–	81.31	–	71.78	–	80.77	–	73.73

Table 3 Raw performance under multi-trial inference. Rows correspond to different trial numbers and the predicted asymptotic convergence value. For each model, we report the average score (Avg) and round-based score (Round). The convergence value is estimated by fitting a saturating exponential model using trial results at $n \in \{1, 2, 4, 8\}$.

Taken together, these results indicate that success on BABE generally requires at least 4–6 inference trials even for frontier models, and 8+ trials for most non-frontier models, highlighting the intrinsic difficulty of experimental reasoning tasks and the limitations of single-pass inference.

5 Conclusion

In this paper, we introduced BABE (Biology Arena BEnchmark), a novel and rigorous benchmark designed to evaluate the experimental reasoning capabilities of large language models in biology. Unlike existing benchmarks that emphasize factual recall, sequence-level prediction, or isolated subtasks, BABE focuses on a core competency of real biological research: integrating experimental results with contextual background to derive scientifically meaningful conclusions.

BABE is constructed entirely from peer-reviewed research papers and real-world biological studies, ensuring that its tasks faithfully reflect the complexity, interdisciplinarity, and ambiguity inherent in actual scientific inquiry. By organizing questions into structured triplets with explicitly defined strong and weak correlation relationships, BABE provides a fine-grained diagnostic framework for assessing both sequential multi-hop reasoning and parallel information extraction within a single source document. This formulation enables more precise identification of reasoning failure modes that are often obscured in conventional benchmarks.

Overall, BABE fills a critical gap in the evaluation of biological AI systems by moving beyond task-level competence toward research-level reasoning. We believe BABE will serve as a valuable testbed for future advances in biologically grounded LLMs, deep research agents, and multimodal scientific reasoning systems. Looking forward, we hope this benchmark will encourage the development of models that reason more like practicing scientists—grounding their conclusions in evidence, maintaining coherence across experimental contexts, and ultimately contributing more reliably to real biological discovery.

References

- [1] Haonan He, Yuchen Ren, Yining Tang, Ziyang Xu, Junxian Li, Minghao Yang, Di Zhang, Dong Yuan, Tao Chen, Shufei Zhang, Yuqiang Li, Nanqing Dong, Wanli Ouyang, Dongzhan Zhou, and Peng Ye. Biology-instructions: A dataset and benchmark for multi-omics sequence understanding capability of large language models, 2025. URL <https://arxiv.org/abs/2412.19191>.
- [2] Jian Huang, Ming Li, and Wei Chen. A systematic review of deep research agents: Architecture, applications, and challenges, 2024. Placeholder entry for a very recent or forthcoming survey.
- [3] Zhen Huang, Zengzhi Wang, Shijie Xia, Xuefeng Li, Haoyang Zou, Ruijie Xu, Run-Ze Fan, et al. Olympicarena: Benchmarking multi-discipline cognitive reasoning for superintelligent ai. *arXiv preprint arXiv:2406.12753*, 2024.
- [4] Zexin Ji, Nayeon Lee, Siffl Frieske, Tiezheng Yu, Dan Su, Yan Xu, Etsuko Ishigaki, Ying Liu, Huaxiu Wen, Yong Liu, et al. Survey of hallucination in large language models. *ACM Computing Surveys*, 56(7):1–38, 2023. doi: 10.1145/3610931.
- [5] J. Jumper, D. Hassabis, et al. Advanced protein structure prediction with AlphaFold3, 2024. Placeholder entry for the latest generation AlphaFold model.
- [6] Tim Kucera, Carlos Oliver, Dexiong Chen, and Karsten Borgwardt. Proteinshake: Building datasets and benchmarks for deep learning on protein structures. In *Advances in Neural Information Processing Systems*, volume 36, 2023. URL https://proceedings.neurips.cc/paper_files/paper/2023/file/b6167294ed3d6fc61e11e1592ce5cb77-Paper-Datasets_and_Benchmarks.pdf. These authors contributed equally.
- [7] Patrick Lewis, Ethan Perez, Aleksandr Piktus, Fabio Fan, Timothée Humeau, Bartłomiej Oglaza, et al. Retrieval-augmented generation for knowledge-intensive nlp tasks. *Advances in Neural Information Processing Systems*, 33: 9459–9474, 2020.
- [8] Zhi Li, Xingyu Zhou, Hao Wang, Chen Zhao, et al. Biobench: A comprehensive benchmark for evaluating large language models in biomedicine, 2024. Placeholder entry for a biomedical reasoning benchmark.
- [9] Joon Sung Park, Joseph C. O'Brien, Carrie J. Cai, Meredith Ringel Morris, Percy Liang, and Michael S. Bernstein. Generative agents: Interactive simulacra of human behavior. *arXiv preprint arXiv:2304.03442*, 2023.
- [10] Yebo Peng, Zixiang Liu, Yaoming Li, Zhizhuo Yang, Xinye Xu, Bowen Ye, Weijun Yuan, Zihan Wang, and Tong Yang. Proof2hybrid: Automatic mathematical benchmark synthesis for proof-centric problems, 2025. URL <https://arxiv.org/abs/2508.02208>.
- [11] Long Phan, Alice Gatti, Ziwen Han, Nathaniel Li, et al. Humanity's last exam. *ArXiv*, abs/2501.14249, 2025.
- [12] Shi Qiu, Shaoyang Guo, Zhuo-Yang Song, Yunbo Sun, Zeyu Cai, Jiashen Wei, Tianyu Luo, Yixuan Yin, Haoxu Zhang, Yi Hu, Chenyang Wang, Chencheng Tang, Haoling Chang, Qi Liu, Ziheng Zhou, Tianyu Zhang, Jingtian Zhang, Zhangyi Liu, Minghao Li, Yuku Zhang, Boxuan Jing, Xianqi Yin, Yutong Ren, Zizhuo Fu, Jiaming Ji, Weike Wang, Xudong Tian, Anqi Lv, Laifu Man, Jianxiang Li, Feiyu Tao, Qihua Sun, Zhou Liang, Yushu Mu, Zhongxuan Li, Jing-Jun Zhang, Shutao Zhang, Xiaotian Li, Xingqi Xia, Jiawei Lin, Zheyu Shen, Jiahang Chen, Qiuhan Xiong, Binran Wang, Fengyuan Wang, Ziyang Ni, Bohan Zhang, Fan Cui, Changkun Shao, Qing-Hong Cao, Ming xing Luo, Yaodong Yang, Muhan Zhang, and Hua Xing Zhu. Phybench: Holistic evaluation of physical perception and reasoning in large language models, 2025. URL <https://arxiv.org/abs/2504.16074>.
- [13] David Rein, Betty Li Hou, Asa Cooper Stickland, Jackson Petty, Richard Yuanzhe Pang, Julien Dirani, Julian Michael, and Samuel R. Bowman. Gpqa: A graduate-level google-proof q&a benchmark. *ArXiv*, abs/2311.12022, 2023.
- [14] Timo Schick, Eric Sch"utze, Vibhav Dwivedi, Joshua de Silva, Ed Wortsman, et al. Toolformer: Language models that can use tools, 2023.
- [15] M-A-P Team, Jiaheng Liu, et al. Supergpqa: Scaling llm evaluation across 285 graduate disciplines. *ArXiv*, abs/2502.14739, 2025.
- [16] George Tsatsaronis, Georgios Balikas, Paris Malakasiotis, et al. BioASQ: A challenge on large-scale biomedical semantic indexing and question answering. *BMC Bioinformatics*, 16(1):1–16, 2015.
- [17] Litu Wang, Yu Chen, Wenlin Ding, Jun Zhu, Bo Wang, et al. A survey on large language model based autonomous agents, 2023.

- [18] Siyuan Weng, Yu Zhang, Yuntian Wang, et al. SciBench: An open-source framework for scientific evaluation of llms, 2023.
- [19] Mingrui Wu, Jiayi Ji, Oucheng Huang, Jiale Li, Yuhang Wu, Xiaoshuai Sun, and Rongrong Ji. Evaluating and analyzing relationship hallucinations in large vision-language models. In Proceedings of the 41st International Conference on Machine Learning, 2024.
- [20] Shunyu Yao, Dianbo Zhao, Mo Yu, Lai Po-Ting, Yejin Hazoom, Abbas Mirhoseini, Wen-tau Hao, et al. React: Synergizing reasoning and acting in language models, 2023.
- [21] Fei Ye, Zaixiang Zheng, Dongyu Xue, Yuning Shen, Lihao Wang, Yiming Ma, Yan Wang, Xinyou Wang, Xiangxin Zhou, and Quanquan Gu. Proteinbench: A holistic evaluation of protein foundation models, 2024. URL <https://arxiv.org/abs/2409.06744>.
- [22] Silong Zhai, Huifeng Zhao, Jike Wang, Shaolong Lin, Tiantao Liu, Shukai Gu, Dejun Jiang, Huanxiang Liu, Yu Kang, Xiaojun Yao, and Tingjun Hou. Peppcbench is a comprehensive benchmarking framework for protein-peptide complex structure prediction. Journal of Chemical Information and Modeling, 65(16):8497–8513, 2025. ISSN 1549-9596. doi: 10.1021/acs.jcim.5c01084. URL <https://doi.org/10.1021/acs.jcim.5c01084>.
- [23] Zehua Zhao, Zhixian Huang, Junren Li, Siyu Lin, Junting Zhou, Fengqi Cao, Kun Zhou, Rui Ge, Tingting Long, Yuexiang Zhu, Yan Liu, Jie Zheng, Junnian Wei, Rong Zhu, Peng Zou, Wenyu Li, Zekai Cheng, Tian Ding, Yaxuan Wang, Yizhao Yan, Tingru Wei, Haowei Ming, Weijie Mao, Chen Sun, Yiming Liu, Zichen Wang, Zuo Zhang, Tong Yang, Hao Ma, Zhen Gao, and Jian Pei. Superchem: A multimodal reasoning benchmark in chemistry, 2025. URL <https://arxiv.org/abs/2512.01274>.

Appendix

A Example Questions of BABE

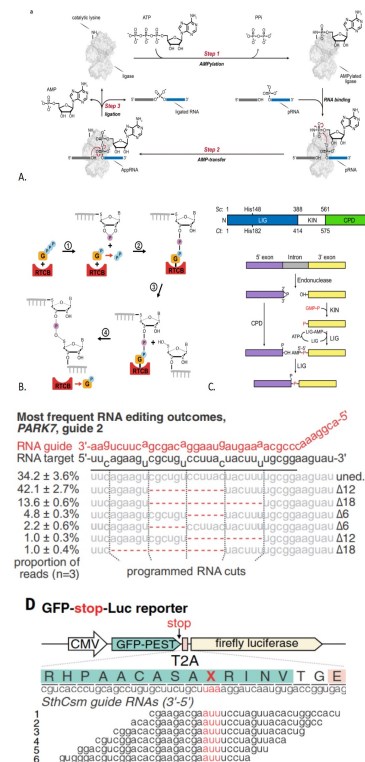
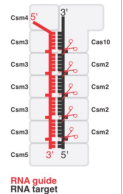
Example Question 1

CRISPR technology was originally used for site-specific DNA cutting and repair (e.g., Cas9), but DNA editing can cause permanent genomic changes and stress responses, posing certain risks. In contrast, targeting RNA allows temporary regulation of gene expression without altering the genome. The Type III-A CRISPR Csm complex is a multi-subunit RNA-targeting endonuclease: guided by gRNA, it only cleaves target RNA. Due to the periodic arrangement of the Csm3 subunit, potential cleavage sites may form every 6 nucleotides in the nucleic acid hybridization region, as shown in [Figure: Case139-1]. The cleaved RNA ends are 5'-OH and 2',3'-cyclic phosphate. The Csm complex enables relatively precise RNA-targeted cleavage and thus holds potential for developing RNA editing technologies. The researchers in this study aim to combine the CRISPR-Csm complex with RNA ligases to achieve RNA fragment deletion via a “cut-and-paste” strategy to repair mis-transcribed transcripts related to human diseases. The following are candidate RNA ligases:

RTCB is a key RNA ligase in mammalian cells, involved in tRNA splicing and the unconventional splicing of XBP1 mRNA during ER stress.

T4 RNA ligase 1 originates from bacteriophage T4, used to repair damaged tRNA during phage infection.

Trl1 is a tRNA ligase unique to fungi and plants that rejoins cleaved exons during tRNA splicing.



<Question 1>:

[Figure: Case139-2] shows the catalytic mechanisms of three RNA ligases: A (T4 RNA ligase 1), B (RTCB), and C (Trl1). Among them, which one is most suitable for the current research design (disregarding species specificity and catalytic complexity)? Note: LIG, KIN, and CPD are different domains of Trl1.

<Question 2>:

After selecting the appropriate RNA ligase, the researchers used PARK7 (related to Parkinson’s disease) as a model transcript and designed corresponding gRNAs to perform RNA “cut-and-paste” experiments. [Figure: Case139-3] shows the proportions of various transcript types obtained after intracellular PARK7 mRNA was reverse-transcribed and sequenced using flanking primers. Assuming all edited products were formed by ligation after cleavage at two sites, please rank the five possible cut sites (labeled 1 to 5 from left to right) in order of cleavage frequency from highest to lowest.

<Question 3>:

To verify whether the Csm complex can restore downstream protein translation by deleting a stop codon on mRNA, the researchers designed the following experiment: PEST is a degradation signal sequence to enhance fluorescence sensitivity; T2A is a short peptide that causes ribosomal skipping between Gly and Pro, allowing independent expression of two genes; SthCsm is a specific Csm complex. Five guide RNAs were designed (shown in [Figure: Case139-4] as 1, 2, 3, 4, 5). Assuming that the cleavage frequency at each site remains constant across different gRNA sequences, which two gRNAs are theoretically expected to yield the highest relative luciferase activity? Please analyze the reason.

Answer

<Question 1> Answer: The respondent only needs to judge that RTCB should be selected.

<Question 2> Answer: 2>4>5>3>1.

<Question 3> Answer: gRNA3, 4.

Subject: Biotechnology and Methodology

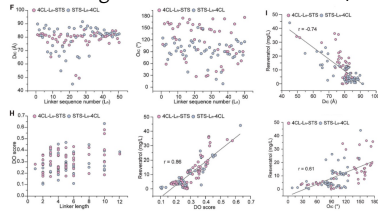
Figure 4 Example Question 1 of BABE

Example Question 2

The efficient assembly of artificial multi-enzyme complexes has been a challenge in the field for many years. How can two enzymes within the same metabolic pathway be effectively linked to improve yield? Researchers established the following model: Alphafold structure prediction → identification of structural features directly related to yield → guidance for designing linkers.

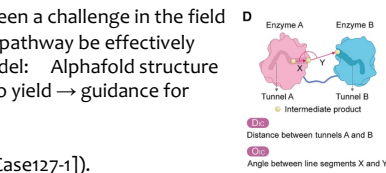
Dic: the distance between the two enzyme channels;

Oic: the angle between the illustrated X/Y segments (see [Figure: Case127-1]).



<Question 1>:

The researchers aimed to find a simple indicator to predict the effect of linkers on yield improvement. They therefore analyzed the relationships among several structure-predicted parameters and their correlation with the actual production of resveratrol, as shown in [Figure: Case127-2]. Which indicator best suits the researchers' purpose (choose among DO score, Oic, and Dic)?



<Question 2>:

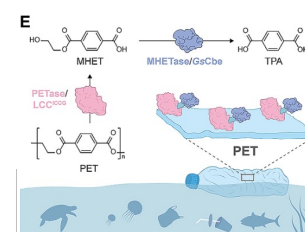
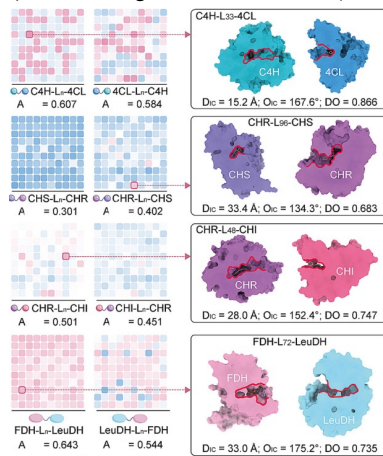
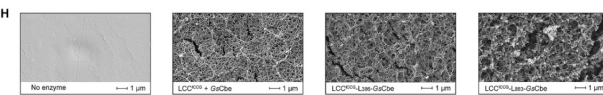
The key indicator obtained above was designated as Indicator A. As shown in [Figure: Case127-3], a heatmap displays the values of Indicator A for fusion enzymes containing different linkers, as well as their average values (written below each matrix group). Based on this figure, answer the following:

To obtain potentially high-yielding fusion proteins, which color of fusion proteins should be prioritized in [Figure: Case127-3] (bluish, white, or reddish)?

Assuming Indicator A is a universally reliable predictor, do you expect the order of enzyme fusion to influence yield? <Question 3>:

PETase (or LCC ICCG) is a class of enzymes capable of acting on PET polymer chains, degrading PET into the intermediate product MHET (mono(2-hydroxyethyl) terephthalate).

Subsequently, MHETase (or GsCbe) further hydrolyzes MHET to produce the final product TPA (terephthalic acid), as shown in [Figure: Case127-4]. The researchers applied the above strategy here and screened efficient fusion proteins. SEM images of plastic films treated with different proteins are shown in [Figure: Case127-5]. Which protein (or protein combination) produced the best effect?



Answer

Answer to <Question 1>: DO score;

Answer to <Question 2>: (1) Slightly reddish; (2) Exists an impact;

Answer to <Question 3>: LCC ICCG-L883-GsCbe

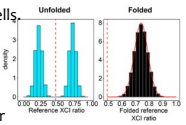
Subject: Biochemistry and Metabolic Biology

Figure 5 Example Question 2 of BABA

Example Question 3

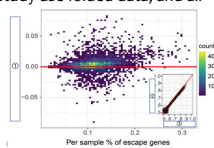
During early human embryonic development, random X-chromosome inactivation (XCI) occurs in different cells. The progeny of these cells maintain the same inactive X chromosome, meaning that the choice of which X chromosome is inactivated does not change afterward. We define the proportion of maternal X chromosome copies that are inactivated in somatic cells as the XCI ratio. Researchers are highly interested in factors that influence XCI and conducted the following study. (Note: In this study, we completely ignore the possibility that the inactivated X chromosome may change after XCI has been established.)

Researchers used SNPs inherited from the parents to calculate XCI ratios and obtained distributions such as shown in [Figure: Case161-1]. These raw distributions are not convenient for analysis, so the authors developed a “fold” method, which disregards the direction of imbalance and only focuses on the deviation from 0.5. All SNP reference allele proportions (Reference XCI ratio) are folded to be above 0.5 to produce the Folded reference XCI ratio. For example, if a SNP has a Reference XCI ratio of 0.2, its Folded reference XCI ratio becomes 0.8. [Figure: Case161-1] shows examples before and after the fold. All subsequent figures in this study use folded data, and all mentions of Folded reference XCI ratio are abbreviated as XCI ratio.



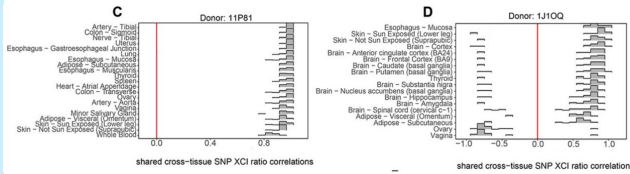
<Question 1>: The presence of “escape genes” may affect the estimation of overall XCI, because these genes are expressed from both the inactive and active X chromosomes. To assess the impact of escape genes, the authors calculated XCI ratios with escape genes removed (XCI ratio with escape) and without removing them (XCI ratio), based on sample SNPs, and produced [Figure: Case161-2]. Carefully examine [Figure: Case161-2] and infer what should be filled in positions ①, ②, and ③ in panel F.

(Note: ① is the y-axis of the large plot; ② is the y-axis of the small plot; ③ is the x-axis of the small plot.)



<Question 2>:

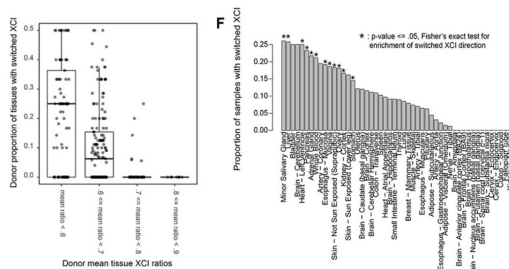
After a series of studies, the authors concluded that the determination of overall XCI in an individual occurs before germ layer differentiation, approximately when the embryo has only 6–16 cells. Because different tissues from the same individual share the same heterozygous SNPs, for a given heterozygous SNP, the reference allele in all tissues of the same individual comes from the same parental chromosome (either always paternal or always maternal), allowing inference of the “direction” of XCI (i.e., which X chromosome is inactivated). During the study, the authors observed that different tissues of the same individual may undergo XCI direction switching. To detect in which tissues this occurs, they developed a method: for a donor, all tissues are paired, and the Pearson correlation coefficient of reference allele ratios across all shared heterozygous SNPs is calculated. [Figure: Case161-3] shows results for two donors in violin plot format. Determine whether donors 11P81 and 1J1OQ have tissues with XCI direction switching, and if so, identify the specific tissue(s) involved.



<Question 3>:

The authors further found that the probability of XCI direction switching is associated with the individual's XCI ratio, as shown in [Figure: Case161-4], panel E. They also found that the probability of XCI direction switching differs among tissues. They then calculated the frequency of XCI direction switching across all donors for each tissue ([Figure: Case161-5]), and statistical testing revealed that some tissues have significantly higher frequencies (indicated by **). Based on your understanding of XCI direction switching, what is the likely core factor that explains why these tissues have higher frequencies of XCI direction switching?

(Note: When selecting donors, no restriction was made on XCI ratio, meaning that XCI ratios may differ between donor pairs.)



Answer

Answer to <Question 1>: ①: XCI ratio – XCI ratio with escape; ②: XCI ratio with escape; ③: XCI ratio

Answer to <Question 2>: Donor 11P81 has none, donor 1J1OQ's Ovary and Vagina experienced an “XCI direction switch” event.

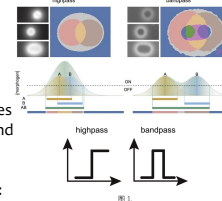
Answer to <Question 3>: Core commonality: These tissues all develop from smaller progenitor cell pools, meaning they have fewer progenitor cells.

Subject:Developmental Biology

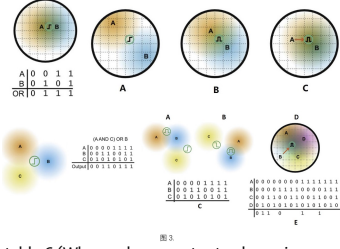
Figure 6 Example Question 3 of BABA

Example Question 4

Biocomputing is a highly promising field with potential applications in biosafety, environmental monitoring, and personalized medicine. Researchers have designed a novel colony-level logic gate system inspired by diffusible morphogen-like signaling during individual development. In this system, computing colonies (i.e., engineered *E. coli* containing logic gate circuits) are inoculated onto agar plates to form individual colonies that can sense signal molecules at other locations on the same agar plate and produce a corresponding output signal (fluorescent output). By combining different logic gate circuits and varying the spatial arrangement of colonies and signal molecule droplet positions, researchers can create complex logic gates and even perform simple binary arithmetic operations. As shown in [Figure: Case100-1], two droplets of signal molecules are applied onto the agar plate, and due to diffusion in the solid medium, different concentration gradients form. The combination of signal droplet positioning and colony distribution enables the construction of different logic gates.



<Question 1>: Researchers designed logic gates on an agar plate as shown in [Figure: Case100-2], where the large black circles represent agar plates, green-bordered circles represent engineered *E. coli* colonies, and the symbols in the center of the green-bordered circles represent high-pass and band-pass behaviors (same as in [Figure: Case100-1]). In signal processing, two common concepts appear: high-pass and band-pass. As the names suggest, high-pass indicates an output signal is generated only when the input reaches a certain threshold, while band-pass requires the input signal to fall within a specific range—too low or too high will not generate output. A and B represent the droplet points of two input signal molecules, and the orange and blue gradient circles centered on AB represent the diffusion ranges of the signal molecules. [Figure: Case100-3] (left) shows an OR gate example with a truth table below, where 0 means no input (no droplet applied), and 1 means an input is present. What types of logic gates do images A, B, and C in [Figure: Case100-2] (right) represent?



<Question 2>: Beyond dual-input systems, this setup can be extended to three- or even four-input systems as shown in Figure 3. The system can also use two output colonies to increase complexity. In [Figure: Case100-3], the left image illustrates a three-input, single-output computing system. A three-input system can be decomposed into two nested logic gates. For example, in the left image, A and C form an AND gate, which is then combined with B to form an OR gate. Based on the examples, write out the output computation results for two three-input, dual-output systems (A and B) for truth table C (When only one output colony gives a result of 1, the final result is 1; when both output colonies yield 1 simultaneously, the result is also considered 1. Note: the colony near the C signal droplet in diagram B is a low-pass colony, which functions opposite to high-pass).

Also, deduce the missing computation results in D based on the partially given four-input truth table in E.

Finally, based on the examples, write the logic gate names (or logical expressions) for systems A, B, and D (e.g., (A AND C) OR B).

<Question 3>:

To achieve binary addition and subtraction, researchers integrated and modified relevant genetic circuits, creating a three-input, dual-output genetic circuit as shown in [Figure: Case100-5]. Its input signal is the 3OC8 AHL molecule, and the output is the 3OHC14:1 AHL molecule. In the blue box on the right, the *Pcon* promoter is a constitutive promoter that drives expression of *tetR*, which binds the *tetO* sequence and inhibits downstream *CinI* expression. Due to the presence of *tetR*, *CinI* in the blue box is only expressed when the input signal concentration reaches the highest level corresponding to three inputs.

What is the resulting truth table for the gene circuit shown in [Figure: Case100-4] (as indicated in [Figure: Case100-5])?

Input 1	0	1	0	0	1	1	0	1
Input 2	0	0	1	0	1	0	1	1
Input 3	0	0	0	1	0	1	1	1

图 5.

Answer

Answer to <Question 1>:

Figure A: AND gate, Figure B: XOR gate, Figure C: NIMPLY gate or (NOT A) AND E

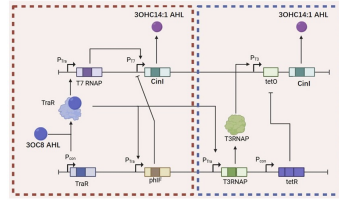


图 4.

Answer to <Question 2>:

A system output: 00111101

A system logical expression: (A XOR B) OR (B AND C)

B system output: 10101100

B system logical expression: NOT (C AND (B OR (NOT A)))

C system output (only the blank areas): 1 000 11 0000

C system logical expression: (A OR C OR D) AND NOT B

Answer to <Question 3>:

The truth table output result is: 0111000

Subject: Biotechnology and Methodology

Figure 7 Example Question 4 of BABA

Example Question 5

Researchers developed a novel method to detect DNA replication origins and termini, called OK-seq. The main principle is to sequence Okazaki fragments to determine the direction of replication fork movement in a genomic region, allowing identification of replication start and end sites.

<Question 1>:

Researchers defined the RFD (Replication Fork Directionality) value to indicate replication fork movement:

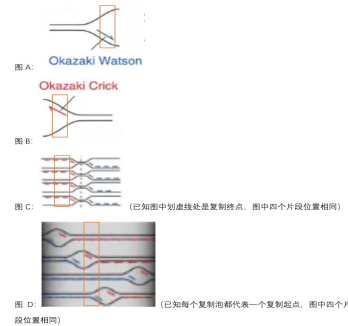
$$RFD = R - L$$

where R is the proportion of forks moving to the right (downstream) and L is the proportion moving to the left (upstream). RFD ranges from -1 to 1. Considering only the replication fork movements shown in [Figure: Case167-2] (panel a), what is the RFD value in the orange-boxed regions of [Figure: Case167-1]?

(Options: ① RFD = 1; ② RFD = 0; ③ RFD = -1; ④ $-1 < RFD < 0$ or $0 < RFD < 1$)

In [Figure: Case167-1], panel C: the dashed line indicates a replication termination site; the four fragments are aligned.

In [Figure: Case167-1], panel D: each replication bubble represents a replication origin; the four fragments are aligned.



Question 2>:

Researchers further examined the RFD patterns at replication origins and termini. Considering initiation and termination timing during early and late S phase, for the replication region shown in [Figure: Case167-2] (panel a), which images in [Figure: Case167-3] and [Figure: Case167-4] best match the expected OK-seq results?

(Y-axis: RFD; X-axis: chromatin physical position; horizontal black line: RFD=0)

<Question 3>:

Based on your choice in <Question 2>, what type of RFD curve should researchers detect to identify replication origin regions?

(Options: A. Upward sloping; B. Downward sloping; C. Horizontal; D. Vertical upward; E. Vertical downward)

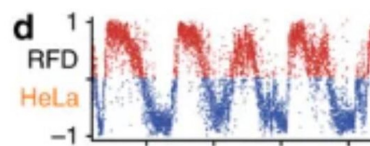
According to your assessment and [Figure: Case167-5] (panel d), how many replication origin regions are displayed in [Figure: Case167-5] (panel d)?

Answer

Answer to <Question 1>: -1 1 1 0

Answer to <Question 2>: Figure 3 and Figure 5.

Answer to <Question 3>: A 5 (or 6).



Subject: Molecular Biology

Figure 8 Example Question 5 of BIBE

Example Question 6

The researchers studied the activity of dopamine neurons in monkeys as they made choices.
<Question 1>:

In each experiment, the monkey needs to make a choice based on the prompt. If the choice is correct, it hears a sound indicating correctness and receives a reward. If incorrect, it hears a sound indicating error. During this period, the researcher records the activity of the dopamine neurons in the monkey's midbrain. "Correct" and "Error" represent the correct/incorrect choices that the monkey will make or has already made. What do the white dashed lines to the right of the left and right images in [Figure: Case145-1] represent in terms of neuronal activity during which periods?

(Available options: ① when the monkey receives the prompt; ② after the monkey receives the prompt and before making the choice; ③ when the monkey hears the sound indicating correctness/incorrectness)

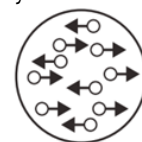
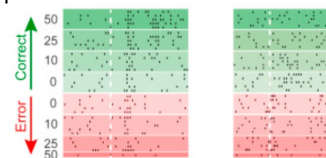
<Question 2>:

It is known that the numbers in the figure of <Question 1> represent the "coherence" of the prompt. The researchers provided the monkey with prompts as shown in [Figure: Case145-2]. The greater the coherence, the more uniform the direction of the small dots in the prompt. The monkey needs to choose to look left or right based on the prompt, and if the direction matches the prompt, it is considered correct. Based on Question (1), what is the relationship between dopamine neuron activity frequency and coherence when "the monkey receives the prompt"?

(Available options: ① positive correlation; ② negative correlation; ③ no significant correlation; ④ initially negative correlation followed by positive correlation as coherence increases; ⑤ initially positive correlation followed by negative correlation as coherence increases)

<Question 3>:

Based on the previous figures and conclusions, if the neuronal activity frequency difference is not significant when the monkey hears the sound indicating correctness or error after making a decision, which prompt from [Figure: Case145-3], [Figure: Case145-4], and [Figure: Case145-5] is most likely displayed in front of the monkey?



Answer

Answer to <Question 1>:

Left image, right side of the white dashed line: ①, ②

Right image, right side of the white dashed line: ③

Answer to <Question 2>: ③

Answer to <Question 3>: A

Subject: Evolutionary Biology and Ethology

Figure 9 Example Question 6 of BABE

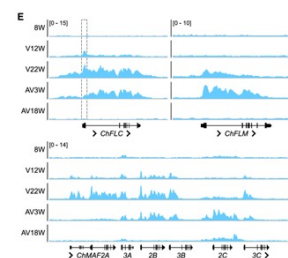
Example Question 7

Researchers identified several genes in *Arabidopsis* that are closely associated with flowering and vegetative growth. Please answer the following questions:

<Question 1>:

[Figure: Case158-1] shows the expression of a series of genes at different time points. Here, “8W” represents 8 weeks of growth at room temperature; “V12W” represents week 12 of growth with a shift to low temperature; “V22W” represents week 22 with a shift to low temperature; “AV3W” represents week 3 after cold treatment; “AV18W” represents week 18 after cold treatment. Z-score measures changes in RNA expression levels of each gene, and CPM represents counts per million. Based on previous studies, it is known that these genes regulate flowering through their expression changes.

Here, we assume that all flowering-promoting or flowering-repressing genes have the same effect strength at equal expression levels. Both species in the figure require vernalization to flower. What is the effect of FLC, FLM, MAF2A, and MAF3A genes on flowering in the two species? (Options: ① Promote flowering / ② Repress flowering / ③ Effect not significant)



<Question 2>:

To further validate the conclusions from <Question 1>, researchers conducted a series of experiments. One experimental result is shown in [Figure: Case158-2] (panel F). What is this experiment most likely measuring?

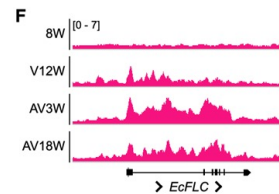
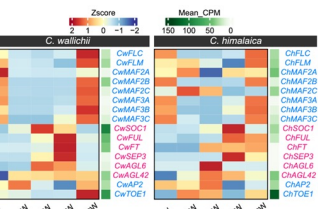
(Hint: The labels under each figure—“ChFLC,” “ChFLM,” “ChMAF2A,” “3A,” etc.—indicate the corresponding genes; black vertical lines represent exon regions.)

<Question 3>:

[Figure: Case158-3] shows measurements for another *Arabidopsis* plant, using the same metric as in <Question 2>. Based on the data, what type of plant is this *Arabidopsis* plant? If it is known to be an annual plant, which part of FLC is altered and how? (Options: ① Mutation in transcription factor binding region, preventing repression; ② Mutation in transcription factor binding region, preventing activation; ③ Exon mutation, resulting in loss of protein function; ④ Exon mutation, resulting in gain of protein function)

*Remark:

- ① Annual (flowers once within one year)
- ② Biennial (does not flower in the first year; flowers in the second year after cold treatment)
- ③ Perennial (flowers multiple times)
- ④ Non-flowering (maintains population via vegetative propagation)*



Answer

Answer to <Question 1>:

FLC, FLM, MAF2A: Inhibit flowering

MAF3A: No significant effect.

Answer to <Question 2>:

Epigenetic modifications that suppress transcription (or detailed responses like suppressive modifications such as H3K27me3, chromatin compaction, etc. can also be provided. "Openness" cannot be used as it contradicts the phenomenon described in <Question 1>).

Answer to <Question 3>:

Biennial. Exon mutation leading to loss of protein function.

Subject: Plant Science

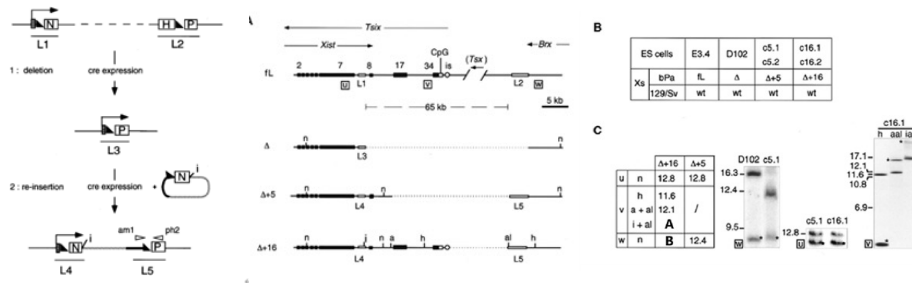
Figure 10 Example Question 7 of BABE

Example Question 8

In the process of X-chromosome inactivation, one X chromosome in each female embryo cell is randomly selected, coated by Xist RNA, and silenced. *Tsix* is the antisense transcript of *Xist*, which participates in the selection of the inactive X and the regulation of *Xist* through an unknown mechanism. Undifferentiated female embryonic stem cells have two active X chromosomes, and X chromosomes are randomly inactivated during induced differentiation. In a female embryonic stem cell line, a 65kb deletion, including the terminal of the *Xist* gene and the starting point of *Tsix*, results in the non-random inactivation of the 65kb-deleted X chromosome in differentiated embryonic stem cells. Below is a study on the function of *Tsix*.

<Question 1>:

As shown in [Figure: Case184-1], the researchers used the knockout and re-insertion method mentioned in the previous question to construct the four X chromosomes shown in [Figure: Case184-2]. Panel B in [Figure: Case184-3] shows the established cell lines, where bPa and 129/Sv are the cell line names. Panel C in [Figure: Case184-3] shows the Southern Blot verification. The n, i, a, al in the figure are the enzyme cutting sites, and u, v, w are the hybridization fragments. The band marked with an asterisk (*) is the hybridization band corresponding to the X chromosome in the 129/Sv cell line. How many additional kb bases are inserted in $\Delta+5$ compared to Δ ?

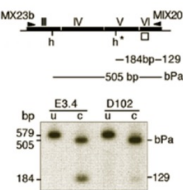


<Question 2>:

What is the closest value to B in the table of panel C in [Figure: Case184-3]?

<Question 3>:

[Figure: Case184-4] shows the detection results of Xist expression products in the E3.4 and D102 cell lines. h represents the HindIII enzyme cutting site, RT-PCR was used for amplification, and Southern Blot was used for color development to obtain results. u and c represent uncut and cut, respectively. The white box indicates the fragment corresponding to the probe used for hybridization. What is the distance between the two HindIII enzyme cutting sites?



Answer

Answer to <Question 1>: 8.9Kb

Answer to **Question 18.5**:

Answer to **Question 29**: 24.5

Subject: Cell Biology

Figure 11 Example Question 8 of BABE